Chapter 5

Solution to the low wavenumber problem

5.1 Overview

The previous chapter illustrated the elastic inversion algorithm using synthetic and field data inversions. One conclusion was that the low-wavenumber components of the velocity converged slowly when inverting reflection seismic data suggesting low wavenumbers were pooly resolved. This chapter proves that the low wavenumbers *can* be resolved and suggests how to speed their convergence to match that of the high-wavenumbers. I restrict the development to the acoustic case to simplify the mathematics. All concepts and conclusions apply to the elastic case as could be seen by replacing acoustic Green's functions with elastic Green's functions.

The inversion algorithm given in chapter 3 is equivalent to doing an iterative migration and diffraction tomography simultaneously. Diffraction tomography and inversion work best when sources and receivers surround the region of interest, as in medical imaging applications. Typical analyses of inversions using seismic reflection data indicate that the high vertical wavenumber velocity perturbations should be resolvable while low wavenumbers should be unresolvable. Therefore, it was thought that the low vertical wavenumbers had to be supplied to inversions using a separate step such as a velocity analysis or reflection tomography (as was done in the previous chapter). In this chapter, I will show that the iterative elastic inversion *obtains all wavenumbers* that are resolvable separately by velocity analysis, migration and reflection tomography. Reflectors in the background

model simulate sources and receivers within the Earth so the source and receiver coverage in seismic reflection inverse problems is effectively the same as in medical imaging. Some synthetic examples verify the theoretical predictions and show that reflector locations and interval velocities can be obtained simultaneously.

5.2 What is the low wavenumber problem?

5.2.1 The problem

Typical analyses of the seismic inverse problem with sources and geophones on the Earth's surface show that the velocity image will only be partially reconstructed (Devaney, 1984; Devaney and Beylkin, 1984; Esmersoy et al., 1985; Esmersoy and Levy, 1986; Wu and Toksöz, 1987). In particular, only the high vertical wavenumbers are resolved and inversion results look like migration results and do not resolve, but rather require, a smooth (low-wavenumber) velocity model (Mora, 1987c).

5.2.2 The problem with the problem

However, it is well known that routine velocity analysis and reflection tomography make use of the shapes of reflection hyperbolas to obtain the low-wavenumber velocity model, so the low-wavenumber information *is* contained in the seismic wavefield. Why does it seem that inversion fails to obtain the low wavenumbers? This question is especially perplexing considering inversion purports to obtain a velocity model that generates synthetic data that best matches the observed seismic wavefield including the hyperbola shapes.

5.2.3 Resolution of the problem through assumptions

Before answering the question of the apparently unresolvable low-wavenumbers, first recall that velocity analysis and tomography both make specific assumptions that enable them to resolve the low wavenumber information. For instance, velocity analysis assumes flat reflectors (and straight rays => small offsets) and tomography often makes specific assumptions about the reflectors (for example that the reflectors have been identified or that reflectors are flat or continuous).

5.2.4 Resolution of the problem through inversion in principle

An inversion that best matches the observed seismic wavefield to a synthetic wavefield should obtain all wavenumber components in a velocity model. To account for the shapes of reflection hyperbolas, the low-wavenumber velocity model must be correct. To account for reflection amplitudes the high-wavenumber velocity model must be correct. What is the problem with the analyses indicating that these low wavenumbers cannot be obtained? Or is it a problem in the inversion algorithms themselves?

5.2.5 Resolution and understanding through analysis

An analysis of an acoustic inversion using a *non-constant* background model containing a deep reflecting interface shows that *all* wavenumbers can be resolved up to some maximum value. This value depends on the maximum frequency in the seismic wavelet. Therefore, provided the inversion assumes a background model that is *non-constant* and contains the reflector locations, the inversion is capable of resolving all wavenumbers. Considering the first iteration of an iterative inversion locates the reflectors, it is not really necessary to know the reflector locations a priori. Consequently, an *iterative* inversion that allows both the *high- and low-wavenumber components of the background model to vary* is a *complete* inversion. In other words, it resolves both reflector locations as well as interval velocities simultaneously. Although the analysis is done for the inversion algorithm restricted to an acoustic medium, the same conclusion applies to elastic waves. Green's functions would be elastic rather than acoustic in the development and P- and S-wave interval velocities and reflector locations would be obtained.

5.3 Are the low wavenumbers resolvable?

5.3.1 Insights from pictures

The chapter on elastic inversion theory showed some pictures describing how the least squares gradient direction was computed. Two wave simulations were required, a forward simulation to model waves in the current estimate of the Earth model and a back propagation of the data residuals.

The pictures illustrating inversion of transmission data showed that the two wave simulations contained waves traveling in the same direction and interval velocities were

resolved. The inversion behaved like a wave-equation tomography! However, the pictures illustrating inversion of reflection data showed that when the two wavefields contained waves traveling in the opposite directions, only the reflectivities were resolved. But both wavefields were computed using the two-way elastic wave equation and thus contained both upgoing and downgoing waves. This suggests that even inversions using only reflection data may be able to resolve interval velocities. This chapter elaborates on this theme.

5.3.2 Non-constant background scattering

I will assume the simplest wave equation, the acoustic wave equation, to simplify algebra. This enables one to focus on the main problem of obtaining high- and low-wavenumber velocity models simultaneously. Of course, all the concepts apply equally well to the full anisotropic elastic wave equation.

Consider the basic plane wave experiment in Figure 5.1.

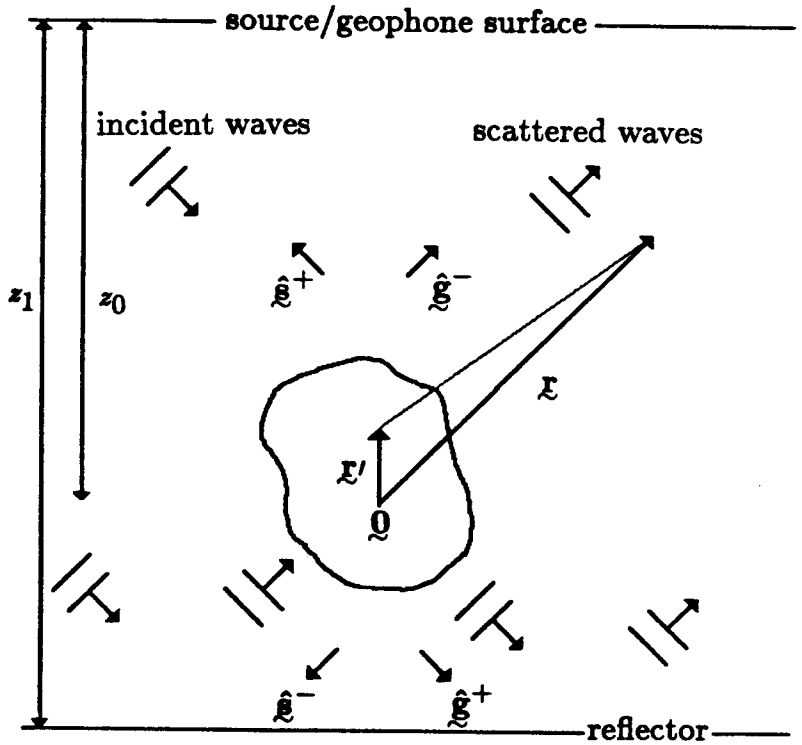

Figure 5.1: Basic plane wave experiment showing plane waves incident on a velocity anomaly embedded in a layer over a halfspace.

A plane wave is incident on a deep anomalous region and a geophone line is located along an absorbing Earth's surface. I assume an absorbing boundary condition to focus the readers attention on primary reflections which I will demonstrate can be used to obtain the low wavenumbers. A simple non-constant background velocity is assumed, namely a layer over a halfspace. It is the presence of the layer-halfspace reflection that enables the low wavenumbers in the velocity anomaly to be resolved in an inversion. This is comparable to the case of reflection tomography but, as we will see in the example, locations of reflectors can be determined by the inversion and are therefore not required a priori.

The following is a derivation of the scattering formulas relating the scattered field to the spectrum of the velocity anomaly (see Wu and Toksöz (1987) for the constant background velocity derivation).

For monochromatic waves, the constant-density acoustic wave equation is

$$\nabla^2 u(\underset{\sim}{r}_s,\underset{\sim}{r}) + \omega^2 W(\underset{\sim}{r}_s,\underset{\sim}{r}) u(\underset{\sim}{r}_s,\underset{\sim}{r}) = f(\underset{\sim}{r}_s) \quad , \tag{5.1}$$

where $u(\underset{\sim}{r}_s,\underset{\sim}{r})$ is the scalar quantity of the wavefield at position $\underset{\sim}{r}$ (such as the pressure), ω is the angular frequency, $f(\underset{\sim}{r}_s)$ is the source function at frequency ω, $\underset{\sim}{r}_s$ is the source position, and $W(\underset{\sim}{r})$ is the squared slowness (i.e. $W(\underset{\sim}{r}) = 1/v^2(\underset{\sim}{r})$ where $v(\underset{\sim}{r})$ is the velocity of acoustic wave propagation). Defining the squared slowness field in the layer to be a background $W_0(\underset{\sim}{r}) = 1/v_0^2(\underset{\sim}{r})$ plus some perturbation $\delta W(\underset{\sim}{r})$,

$$W(\underset{\sim}{r}) = W_0(\underset{\sim}{r})[1 + \delta W(\underset{\sim}{r})] \quad , \tag{5.2}$$

and defining the wavenumber $k = \omega/v_0(\underset{\sim}{r})$ we obtain

$$\nabla^2 u(\underset{\sim}{r}_s,\underset{\sim}{r}) + k^2 u(\underset{\sim}{r}_s,\underset{\sim}{r}) = -k^2 \delta W(\underset{\sim}{r}) u(\underset{\sim}{r}_s,\underset{\sim}{r}) + f(\underset{\sim}{r}_s) \quad . \tag{5.3}$$

Now, by defining the wavefield $u(\underset{\sim}{r}_s,\underset{\sim}{r})$ in terms of the wavefield in the unperturbed medium $u_0(\underset{\sim}{r}_s,\underset{\sim}{r})$ as

$$u(\underset{\sim}{r}_s,\underset{\sim}{r}) = u_0(\underset{\sim}{r}_s,\underset{\sim}{r}) + \delta u(\underset{\sim}{r}_s,\underset{\sim}{r}) \quad , \tag{5.4}$$

and applying the Born approximation, namely that higher order terms can be neglected, and applying equation (5.1) yields

$$\nabla^2 \delta u(\underset{\sim}{r}_s,\underset{\sim}{r}) + k^2 \delta u(\underset{\sim}{r}_s,\underset{\sim}{r}) = -k^2 \delta W(\underset{\sim}{r}) u_0(\underset{\sim}{r}_s,\underset{\sim}{r}) \quad . \tag{5.5}$$

The solution to this equation in terms of the acoustic wave equation Green's functions for the medium $G(\underset{\sim}{r}',\underset{\sim}{r})$ is

$$\delta u(\underset{\sim}{r}_s,\underset{\sim}{r}) = \int_V k^2 \delta W(\underset{\sim}{r}') u_0(\underset{\sim}{r}_s,\underset{\sim}{r}') G(\underset{\sim}{r}',\underset{\sim}{r}) d\underset{\sim}{r}' \tag{5.6}$$

$$= \int_V k^2 \delta W(\underset{\sim}{r}') G(\underset{\sim}{r}_s, \underset{\sim}{r}') f(\underset{\sim}{r}_s) G(\underset{\sim}{r}', \underset{\sim}{r}) d\underset{\sim}{r}' \quad . \tag{5.7}$$

So far the discussion has been valid for sources located without restriction at $\underset{\sim}{r}_s$ and geophones at $\underset{\sim}{r}$. Now, restricting the sources and geophones to be located on the Earth's surface yields

$$\delta u(x_s, x_g) = \int_V k^2 \delta W(\underset{\sim}{r}) G(x_s, \underset{\sim}{r}) f(x_s) G(x_g, \underset{\sim}{r}) d\underset{\sim}{r} \quad . \tag{5.8}$$

Note that the Green's functions obey reciprocity between source and geophones, namely that $G(\underset{\sim}{r}', \underset{\sim}{r}) = G(\underset{\sim}{r}, \underset{\sim}{r}')$. Fourier transforming over the source location x_s and geophone location x_g yields

$$\delta \tilde{u}(k_s, k_g) = \int_V k^2 \delta W(\underset{\sim}{r}) \tilde{G}(k_s, \underset{\sim}{r}) \tilde{f}(k_s) \tilde{G}(k_g, \underset{\sim}{r}) d\underset{\sim}{r} \quad . \tag{5.9}$$

So far the development assumed nothing about the Green's functions and hence nothing about the background medium $W_0(\underset{\sim}{r})$. Now, I will assume the simplest inhomogeneous non-smooth background medium, namely a layer over a halfspace. Furthermore, I will assume the anomaly region is above the interface between the layer and halfspace (see Figure 5.1). In that case, the approximate Green's functions for the background medium are

$$\tilde{G}(k_s, \underset{\sim}{r}) = \tilde{G}^+(k_s, \underset{\sim}{r}) + \tilde{G}^-(k_s, \underset{\sim}{r})$$

$$= \frac{i}{2} \frac{\exp(i\gamma_s d_s^+)}{\gamma_s} \exp(-ik\underset{\sim}{\hat{s}}^+ \cdot \underset{\sim}{r}) + \tilde{c}(k_s) \frac{i}{2} \frac{\exp(i\gamma_s d_s^-)}{\gamma_s} \exp(-ik\underset{\sim}{\hat{s}}^- \cdot \underset{\sim}{r}) \quad , \tag{5.10}$$

and

$$\tilde{G}(k_g, \underset{\sim}{r}) = \tilde{G}^+(k_g, \underset{\sim}{r}) + \tilde{G}^-(k_g, \underset{\sim}{r})$$

$$= \tilde{c}(k_g) \frac{i}{2} \frac{\exp(i\gamma_g d_g^+)}{\gamma_g} \exp(-ik\underset{\sim}{\hat{g}}^+ \cdot \underset{\sim}{r}) + \frac{i}{2} \frac{\exp(i\gamma_g d_g^-)}{\gamma_g} \exp(-ik\underset{\sim}{\hat{g}}^- \cdot \underset{\sim}{r}) \quad , \tag{5.11}$$

where $\underset{\sim}{\hat{s}}$ and $\underset{\sim}{\hat{g}}$ are the unit vectors pointing along the direction of wave propagation away from the origin towards the source and geophone locations, to the source and geophone locations respectively and d_s and d_g are the vertical distances between the origin and the source and geophone lines (the Earth's surface). The superscripts on the Green's functions denote whether the waves are downgoing (+) or upgoing (−) at the origin. The vertical distances traveled by the waves corresponding to each Green's function are denoted d. For instance, d_s^+ is the vertical distance from the source line to the origin (i.e. the anomaly depth) and d_s^- is the vertical distance down to the layer-halfspace interface and back up to

the origin. Specifically, from Figure 5.1, $d_s^+ = z_0$, $d_s^- = 2z_1 - z_0$, $d_g^+ = 2z_1 - z_0$, and $d_g^- = z_0$. Similarly, $\hat{\underset{\sim}{s}}^+$ is the unit vector that points toward the source along a ray that travels in the positive depth direction (downward) while $\hat{\underset{\sim}{s}}^-$ is the unit vector that points toward the source along a ray that travels in the negative depth direction (upward). Thus, the $\hat{\underset{\sim}{s}}^-$ corresponds to the source end of the S^{-+} or S^{--} raypaths shown in Figure 5.2. Likewise, $\hat{\underset{\sim}{g}}^+$ and $\hat{\underset{\sim}{g}}^-$ are unit vectors pointing along the two raypaths between the geophones and the origin. The vertical wavenumbers denoted γ_s and γ_g are specified by

$$\gamma_s = \sqrt{k^2 - k_s^2} \quad , \tag{5.12}$$

and

$$\gamma_g = \sqrt{k^2 - k_g^2} \quad , \tag{5.13}$$

and $\tilde{c}(k')$ is the reflection coefficient of the layer-halfspace interface for an angle of incidence corresponding to wavenumber k and horizontal (shot or geophone axis) wavenumber k'. Notice that waves can travel from the source to the anomaly and then either go up to the geophones or go down to the reflector to be reflected back up to the geophones. These two alternate paths from the anomaly to the geophones are included as two terms in the geophone Green's function $\tilde{G}(k_g, \underset{\sim}{r})$. Similarly, the source Green's function $\tilde{G}(k_s, \underset{\sim}{r})$ describing how waves can get from the source to the anomaly has two components.

The Green's functions are approximate because higher order terms that represent reverberations have been excluded. Also, the sources and geophones were assumed to be located along an absorbing surface whereas the Earth's surface is free resulting in strong multiple scattering terms. Neither of these approximations detract from the following analysis which is simply intended to show that tomographic terms are included in inversion provided the background model generates reflections.

Substituting the approximate Green's functions into equation (5.9) yields the equation for the perturbations of the field variable in terms of the squared slowness anomaly

$$\delta\tilde{u}(k_g, k_s) =$$

$$-\frac{\tilde{f}(k_s)k^2}{4\gamma_s\gamma_g}\left\{\begin{array}{c} \exp(i\gamma_s d_s^+ + i\gamma_g d_g^-)\int_V \delta W(\underset{\sim}{r})\exp[-ik(\underset{\sim}{\hat{s}}^+ + \underset{\sim}{\hat{g}}^-)\cdot\underset{\sim}{r}]d\underset{\sim}{r} \\ +\tilde{c}(k_g)\tilde{c}(k_s)\exp(i\gamma_s d_s^- + i\gamma_g d_g^+)\int_V \delta W(\underset{\sim}{r})\exp[-ik(\underset{\sim}{\hat{s}}^- + \underset{\sim}{\hat{g}}^+)\cdot\underset{\sim}{r}]d\underset{\sim}{r} \\ +\tilde{c}(k_g)\exp(i\gamma_s d_s^+ + i\gamma_g d_g^+)\int_V \delta W(\underset{\sim}{r})\exp[-ik(\underset{\sim}{\hat{s}}^+ + \underset{\sim}{\hat{g}}^+)\cdot\underset{\sim}{r}]d\underset{\sim}{r} \\ +\tilde{c}(k_s)\exp(i\gamma_s d_s^- + i\gamma_g d_g^-)\int_V \delta W(\underset{\sim}{r})\exp[-ik(\underset{\sim}{\hat{s}}^- + \underset{\sim}{\hat{g}}^-)\cdot\underset{\sim}{r}]d\underset{\sim}{r} \end{array}\right\}$$

$$= S^{+-} + S^{-+} + S^{++} + S^{--} \quad . \tag{5.14}$$

Note that there are four scattering terms in this expression are denoted respectively S^{+-}, S^{-+}, S^{++} and S^{--}. Figure 5.2 shows the corresponding raypaths and illustrates the meaning of the superscripts.

The first two terms are the reflection scattering terms. It is these that lead to the resolution of high vertical wavenumbers in the inversion formulas for squared slowness.

In a homogeneous background there would only be one term, the S^{+-} term. This term corresponds to waves that travel down from the source and are scattered by the velocity anomaly back up to the geophones. Therefore, it represents scattering from waves incident from above. Notice that the presence of the deeper reflector has introduced three other terms.

The S^{-+} term corresponds to waves that travel down from the source, reflect up from the layer-halfspace interface, are downward scattered (reflected) from the anomaly back to the interface and are then reflected back up to the geophones.

These last two terms are the transmission scattering terms. It is these that lead to the resolution of the low vertical wavenumbers in the inversion formulas for squared slowness.

The S^{++} term corresponds to waves that travel down from the source, are downward scattered (transmitted) through the anomaly to the interface and then reflected back up to the geophones.

Similarly, the S^{--} term corresponds to waves that travel down from the source, are reflected back up from the layer-halfspace interface and then upward scattered (transmitted) through the anomaly to the geophones.

In other words, the S^{+-} and S^{-+} terms will lead to migration-like terms in the inversion formulas while the S^{++} and S^{--} terms will lead to reflection tomography-like terms. S^{+-} yields the usual migration term, S^{-+} corresponds to back-scattering of waves incident on the anomaly from below so it yields an underside imaging term, and S^{++} and S^{--} correspond to transmission scattering and thus yield tomographic terms. Mora (1987b) gave the corresponding four terms for the case of elastic inversion and suggested how to use these terms to simultaneously resolve both the high and low wavenumbers in the velocity model.

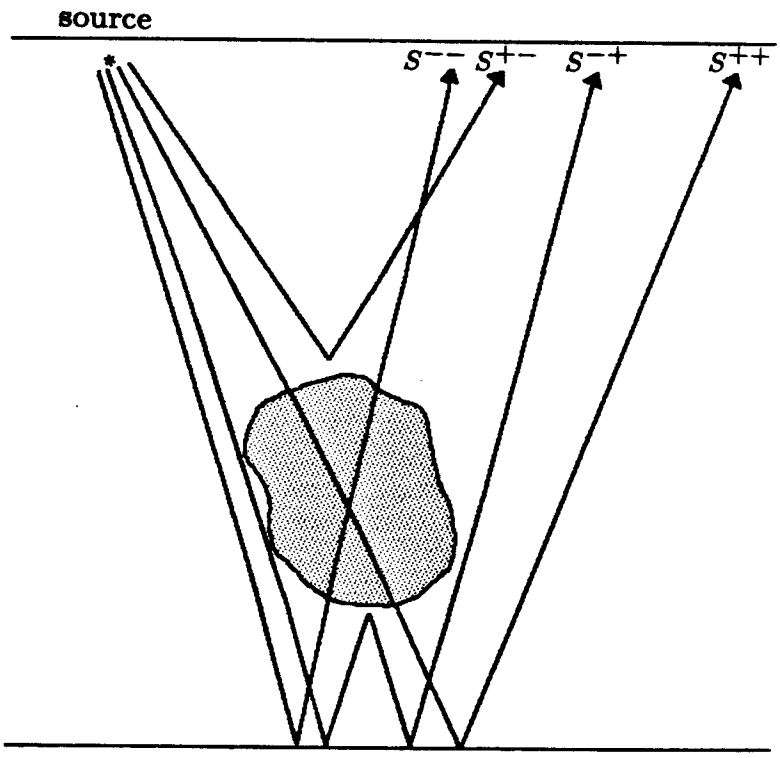

Figure 5.2: Raypaths corresponding to the four different scattering terms. The first superscript refers to the incident ray direction while the second superscript refers to the scattered ray direction (+ is downward and − is upward). For example, S^{+-} has a downgoing incident ray and an upgoing scattered ray.

5.3.3 Non-constant background inversion

Equation (5.14) can be written as

$$\delta\tilde{u}(k_s,k_g) = -\frac{\tilde{f}(k_s)k^2C(\underset{\sim}{\hat{s}})C(-\underset{\sim}{\hat{g}})}{4\gamma_s\gamma_g}\exp[i\gamma_s D_s(\underset{\sim}{\hat{s}})+i\gamma_g D_g(\underset{\sim}{\hat{g}})]\ \times$$

$$\int_V \delta W(\underset{\sim}{r})\exp[-ik(\underset{\sim}{\hat{s}}+\underset{\sim}{\hat{g}})\cdot\underset{\sim}{r}]d\underset{\sim}{r} \quad . \tag{5.15}$$

Now there appears to be only one term because $\underset{\sim}{\hat{s}}$ and $\underset{\sim}{\hat{g}}$ span 360 degrees while previously the $\underset{\sim}{\hat{s}}^+$, $\underset{\sim}{\hat{s}}^-$, $\underset{\sim}{\hat{g}}^+$ and $\underset{\sim}{\hat{g}}^-$ vectors only spanned 180 degrees each. For convenience, I have lumped together reflection coefficient terms like $\tilde{c}(k')$ into $C(\underset{\sim}{\hat{s}})$ and $C(-\underset{\sim}{\hat{g}})$. Similarly, d_s^+ and d_s^- were included in D_s and d_g^+ and d_g^- in D_g. For example,

$$D(\underset{\sim}{\hat{s}}) = \begin{cases} d_s^+ & \textit{when } \underset{\sim}{\hat{s}} \textit{ corresponds to a downgoing ray} \\ d_s^- & \textit{when } \underset{\sim}{\hat{s}} \textit{ corresponds to an upgoing ray} \end{cases} \quad . \tag{5.16}$$

Therefore, equation (5.15) can be considered to be a generic term of equation (5.14). Three dimensional Fourier transformation of equation (5.15) yields the equation for the squared slowness anomaly in terms of the perturbation in the wavefield

$$\delta\tilde{W}[k(\underset{\sim}{\hat{g}}+\underset{\sim}{\hat{s}})] = -\delta\tilde{u}(k_s,k_g)\frac{4\gamma_s\gamma_g}{\tilde{f}(k_s)k^2C(\underset{\sim}{\hat{s}})C(-\underset{\sim}{\hat{g}})}\exp\left\{-i[\gamma_s D_s(\underset{\sim}{\hat{s}})+\gamma_g D_g(\underset{\sim}{\hat{g}})]\right\} \quad . \tag{5.17}$$

Note that I assumed that $C(\underset{\sim}{\hat{e}}) \neq 0$ for all directions $\underset{\sim}{\hat{e}}$ and $\tilde{f}(k_s) \neq 0$ (i.e. the reflection coefficient and source strength are both non-zero for all wavenumbers). Normally, one would apply a small damping term to the denominator to stabilize the solution. Hence, zero's in the source or reflection coefficient at a given wavenumber would result in holes in the wavenumber spectrum for squared slowness.

5.3.4 The resolved wavenumber spectrum

Equation (5.17) relates one plane wave component in the wavenumber spectrum in squared slowness to the wavenumbers of the acoustic waves along the source and geophone axes. Consider the single frequency experiment where the frequency of the source ω is fixed so the length of the vectors $k\underset{\sim}{\hat{s}}$ and $k\underset{\sim}{\hat{g}}$ are constant. Now both $\underset{\sim}{\hat{s}}$ and $\underset{\sim}{\hat{g}}$ span 360 degrees thanks to the reflecting interface between the layer and halfspace (if the interface were not present then we would only have the S^{+-} term and $\underset{\sim}{\hat{s}}$ and $\underset{\sim}{\hat{g}}$ would only span 180

degrees). If we fix $\hat{\underset{\sim}{s}}$ and let $\hat{\underset{\sim}{g}}$ span 360 degrees then a circular zone will be resolved in the wavenumber spectrum of the squared slowness (Figure 5.3).

Now, by letting the source vector $\hat{\underset{\sim}{s}}$ range from 0 to 360 degrees, the entire wavenumber spectrum of the squared slowness will be resolved up to some maximum depending on the frequency ω (Figure 5.4).

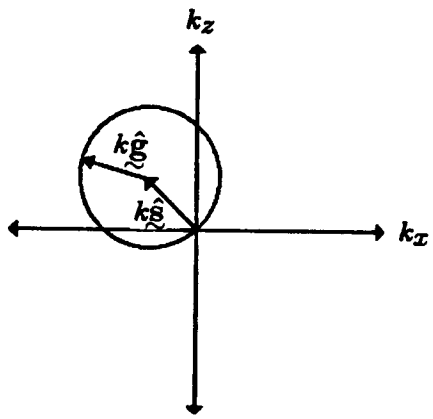

Figure 5.3: The part of the wavenumber spectrum of the squared slowness model that can be resolved using a single plane wave source.

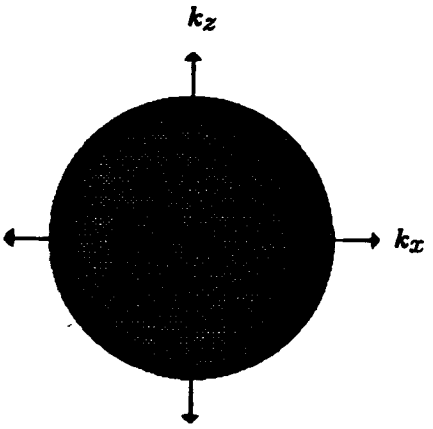

Figure 5.4: The part of the wavenumber spectrum of the squared slowness that can be resolved using a point source (i.e. a sum of plane waves at all angles).

Consequently, when sources and geophones are located on the Earth's surface, a single frequency seismic source will resolve the *entire* wavenumber spectrum of the squared slowness up to a maximum value of $2\omega/v_0$.

To see in detail how the entire squared slowness spectrum is resolved and how the non-constant background relates to the constant background case, I will divide the spectrum into four components. These are derived from the four terms of equation (5.14). Thus, equation (5.17) can be written as the sum of four inversion terms

$$\delta\tilde{W}[k(\underset{\sim}{\hat{s}}+\underset{\sim}{\hat{g}})] \;=\; I^{+-} \;+\; I^{-+} \;+\; I^{++} \;+\; I^{--}$$

$$= \; -\delta\tilde{u}(k_s,k_g)\;\frac{4\gamma_s\gamma_g}{\tilde{f}(k_s)k^2}\left(\begin{array}{c} \exp[-i(\gamma_s d_s^+ + \gamma_g d_g^-)] \\ +\;\frac{1}{\tilde{c}(k_g)\tilde{c}(k_s)}\exp[-i(\gamma_s d_s^- + \gamma_g d_g^+)] \\ +\;\frac{1}{\tilde{c}(k_g)}\exp[-i(\gamma_s d_s^+ + \gamma_g d_g^+)] \\ +\;\frac{1}{\tilde{c}(k_s)}\exp[-i(\gamma_s d_s^- + \gamma_g d_g^-)] \end{array}\right)$$

$$= \; -\frac{\delta\tilde{u}(k_s,k_g)}{\tilde{f}(k_s)k^2}\left(\frac{4\gamma_s\gamma_g}{C(\underset{\sim}{\hat{s}})C(-\underset{\sim}{\hat{g}})}\right)^2 \tilde{G}^*(k_s,k(\underset{\sim}{\hat{s}}+\underset{\sim}{\hat{g}}))\tilde{G}^*(k_g,k(\underset{\sim}{\hat{s}}+\underset{\sim}{\hat{g}})) \quad , \qquad (5.18)$$

where the asterisk denotes conjugate transpose. The division by $\tilde{f}(k_s)$ is deconvolution to remove the source signature and the division of some terms by reflection coefficients allows for the strength of the deeper reflection. As in equation (5.14), the vectors $\underset{\sim}{\hat{s}}^+$, $\underset{\sim}{\hat{s}}^-$, $\underset{\sim}{\hat{g}}^+$ and $\underset{\sim}{\hat{g}}^-$ span 180 degrees each. The first term, the I^{+-} term is the usual homogeneous background term. The part of the squared slowness spectrum resolved by this term is shown in Figure 5.5 (a). It was evaluated at a single frequency ω by letting the vectors $\underset{\sim}{\hat{s}}^+$ and $\underset{\sim}{\hat{g}}^-$ span through the appropriate 180 degree ranges and using symmetry (c.f. Figure 5.4 where $\underset{\sim}{\hat{s}}$ and $\underset{\sim}{\hat{g}}$ both spanned 360 degrees). I also assumed that the velocities were real so there are some symmetry constraints to the wavenumber spectrum (see also Wu and Toksöz (1987)). Similarly, the spectra resolved by the other three terms are also shown in Figure 5.5.

Clearly, the usual homogeneous background term (the I^{+-} term) leaves big holes in the spectrum, particularly in the low vertical wavenumbers. The three extra inhomogeneous background terms fill the rest of the spectrum. In particular, the I^{++} and I^{--} terms

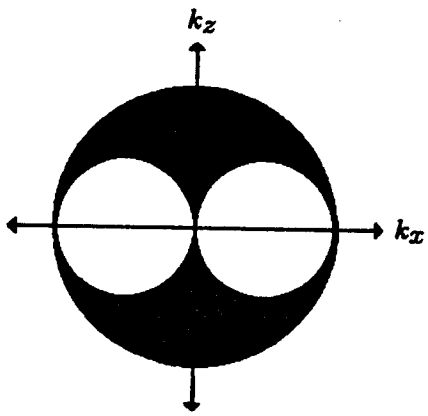

Figure 5.5: (a) The part of the wavenumber spectrum of squared slowness that can be resolved from the I^{+-} inversion term (i.e. the usual imaging term). This is the same as Wu and Toksöz (1987), Figure 12 (a), except that their spectrum was for a wide-band source rather than a single frequency. This is identical to the part of the wavenumber spectrum of squared slowness that can be resolved from the I^{-+} inversion term (i.e. the underside imaging term).

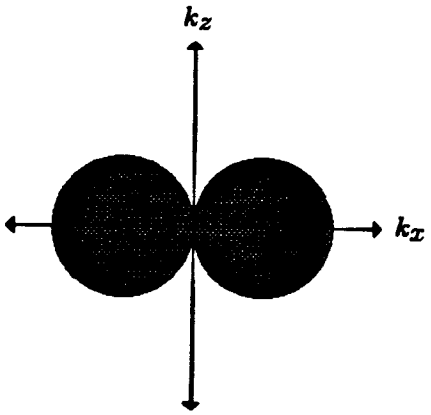

Figure 5.5: (b) The part of the wavenumber spectrum of squared slowness that can be resolved from the I^{++} inversion term (i.e. the downward path tomographic term). This is identical to the part of the wavenumber spectrum of squared slowness that can be resolved from the I^{--} inversion term (i.e. the upward path tomographic term).

fill in the low vertical wavenumbers. Furthermore, the I^{+-} term is the inverse reflection scattering term for waves incident from above while the I^{-+} term is the inverse reflection scattering term for waves incident from below. Similarly, the I^{++} term is the inverse transmission scattering term for waves incident from above while the I^{--} term is the inverse transmission scattering term for waves incident from below (see Figure 5.2 for a ray diagram of the corresponding four scattering terms). Note that I^{+-} and I^{-+} resolve the same part of the wavenumber spectrum. Two holes are in this spectrum in exactly in the place where I^{++} and I^{--} are resolved. Figure 5.5 illustrates the complimentary nature of the I^{+-} and I^{-+} migration-like terms with the I^{++} and I^{--} reflection tomography terms.

5.3.5 The tomographic terms revealed

To illustrate the four inversion terms when the reflector depth is known, consider an inversion of the synthetic data shown in Figure 5.6. It was generated by modeling through a circular velocity anomaly embedded in a layer over a halfspace (Figure 5.7 (a)).

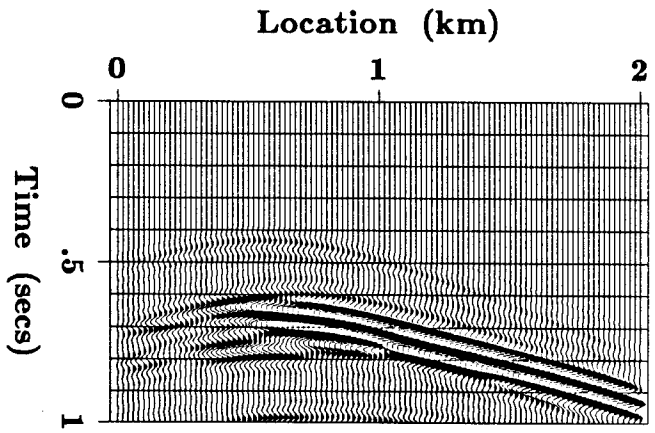

Figure 5.6: Shot gather generated from the model shown in Figure 5.7 (a).

The source wavelet was missing both high and low frequencies being a fourth derivative of a Gaussian curve. An iterative inversion to solve for the velocities was carried out (i.e. equation (5.18) was evaluated). The initial model used in the inversion was a layer over a halfspace. This model was identical with the model that was used to generate the synthetic data except that the circular anomaly was missing from the upper layer. The inversion result (Figure 5.7 (b)) contains the circular anomaly and two weak V shaped features roughly emanating from the source location at zero km and passing through the velocity

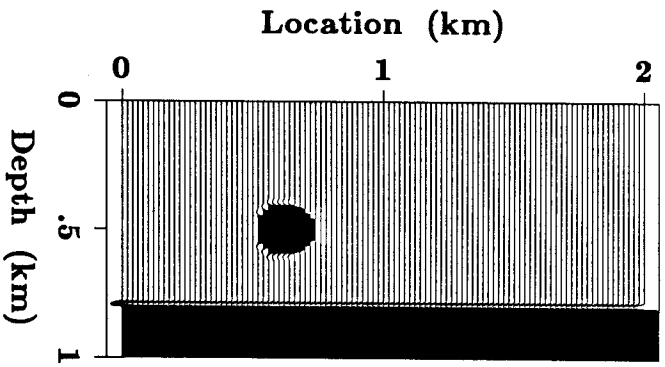

Figure 5.7: (a) The true model corresponding to the synthetic data shown in Figure 5.6. Black depicts a negative perturbation and white a positive perturbation relative to the acoustic impedance in the upper layer. The velocity perturbation of the circular region relative to the layer velocity was 10%.

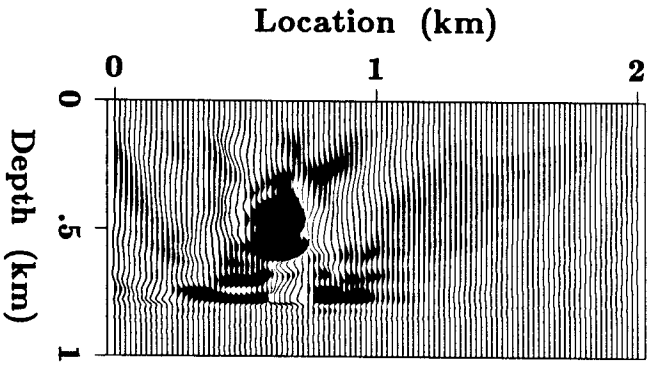

Figure 5.7: (b) Ten iteration inversion result. The starting model was a layer over a halfspace that was identical to the true model except that that the circular velocity anomaly was not present.

anomaly. These V's are the contributions from the tomographic terms I^{++} and I^{--} and look like the ray trajectories for the transmission scattering terms S^{++} and S^{--} shown in Figure 5.2. The migration terms I^{+-} and I^{-+} have sharpened the outline of the circle and slightly repositioned the deeper reflector. The repositioning is seen as a flat event in the inversion result shown in Figure 5.7 (b). If many shot gathers were used in the inversion, the velocity anomaly would have been illuminated from many different directions (just like the human body in medical imaging). Hence a more complete picture (without V's) would be obtained as will be seen in the following example. Only one shot gather was used in this inversion to illustrate the effects of the four different inversion terms. Also, the reflector depth was supplied (i.e. the initial inhomogeneous background velocity consisted of the true layer over the halfspace). The following examples show that iterative inversions do not require knowledge of reflector depth.

5.3.6 Relationship to iterative inversion

Now consider the elastic inversion algorithm derived in Chapter 3. It performs an elastic inversion by conjugate gradient iterations. I will restrict the formulas to the constant density acoustic case (shear velocities equal to zero and density fixed) to simplify the interpretation of the results. The algorithm is based on the elastic wave equation. It attempts to match an observed wavefield with a synthetic wavefield generated by modeling through some velocity model. When the match between the two wavefields is good then the algorithm has converged to the most probable velocity model under the assumptions of least squares (i.e. Gaussian errors in the data and Gaussian distributed velocities). From equation 3.59, the P-wave velocity perturbation at the $(n+1)$-th iteration $\delta v^{n+1}(\underset{\sim}{\mathbf{r}})$ in terms of the data perturbation at the n-th iteration $\delta u^n(x_g,t) = u_0^n(x_g,t) - u_{obs}(x_g,t)$ is

$$\delta v^{n+1}(\underset{\sim}{\mathbf{r}}) \propto \sum_s \int dt\ [\sqrt{t}G^n(x_s,\underset{\sim}{\mathbf{r}},t) * f(x_s,t)][\sum_g \sqrt{t}G^n(x_g,\underset{\sim}{\mathbf{r}},-t) * \delta u^n(x_s,x_g,t)]\ +\ \varepsilon, \tag{5.19}$$

where $u_{obs}(x_g,t)$ is the observed seismic data and $*$ denotes convolution over time, $u(\underset{\sim}{\mathbf{r}}) = \nabla \cdot \mathbf{U}(\underset{\sim}{\mathbf{r}})$ where $\mathbf{U}(\underset{\sim}{\mathbf{r}})$ is the displacement vector and $\varepsilon = C_{vv}^{-1}(v_n - v_0)$ is a damping term. Equation (5.19) is applied iteratively in a conjugate gradient algorithm until the data perturbation is minimized. At this point, synthetic data generated from the velocity model best matches the observed data $u_{obs}(x_g,t)$. For small velocity perturbations and no damping, the iterative time-space domain expression given by equation (5.19) yields exactly

the same solution the frequency-wavenumber domain expression given by equation (5.18). This is easily seen by integrating equation (5.18) over the data space (sources, geophones and frequency) and inverse transforming to the time-space domain

$$\delta W(\underset{\sim}{\mathbf{r}}) \propto \sum_s \sum_g \left[\hat{G}(x_s,\underset{\sim}{\mathbf{r}},-t) * f^{-1}(x_s,t) * \hat{G}(x_g,\underset{\sim}{\mathbf{r}},-t) * \delta u(x_s,x_g,t)\right]_{t=0}$$

$$= \sum_s \int dt[\hat{G}(x_s,\underset{\sim}{\mathbf{r}},t) * f^{-1}(x_s,t)][\sum_g \hat{G}(x_g,\underset{\sim}{\mathbf{r}},-t) * \delta u(x_s,x_g,t)] \quad , \qquad (5.20)$$

where

$$\hat{G} = \frac{G}{|G|} \sim \frac{\sqrt{t}\ cos(\theta)G}{C} \quad , \qquad (5.21)$$

is a normalized Green's function in two dimensions and θ is the angle of wave propagation. Clearly, when restricted to the acoustic case, the equations given in the chapter on elastic inversion theory and rewritten in equation (5.19) are the almost the same as the inversion formulas given in equation (5.20). Differences are:

(i) The Green's functions have been scaled differently because $\sqrt{t}$ = *divergence correction* $\neq$ $1/|G|$ except if incidence angles are small (i.e. $cos(\theta) \approx 1$) and the velocity model is homogeneous (i.e. has no reflectors) so C is unity.

(ii) There is a convolution in equation (5.19) with the source wavelet whereas there is a deconvolution with the source wavelet in equation (5.20),

(iii) Equation (5.19) has a damping term and is applied iteratively.

The conjugate gradient iterations ensure that the synthetic data matches the observed data and hence correct for these differences. To speed the convergence of the iterations, one could easily enough deconvolve rather than convolve with the source wavelet and rescale the Green's functions. In particular, one could allow for the reflection strength by dividing equation (5.19) by the C factor as was done in equation (5.20). Mora (1987b) described this concept and in particular observed that

$$\delta v^{n+1} = [J^{+-} + J^{-+}] + [J^{++} + J^{--}] \sim [I^{+-} + \bar{C}^2 I^{-+}] + \bar{C}[I^{++} + I^{--}] + \varepsilon$$

$$= [\textit{migration} - \textit{like terms}] + [\textit{reflection} - \textit{tomographic} - \textit{like terms}] + [\textit{damping term}] \quad . \tag{5.22}$$

leading to the conclusion that the convergence could be sped up by boosting the reflection-tomographic terms (i.e. J^{++} and J^{--}). Clearly, the boost factor should be about equal to the inverse of the reflection coefficient at a representative angle of incidence denoted $\bar{C}$. Specifically, use in the iterative formula

$$\delta v^{n+1} = [J^{+-} + \frac{1}{\bar{C}^2} J^{-+}] + \frac{1}{\bar{C}}[J^{++} + J^{--}] + \varepsilon \approx 2J^{+-} + \frac{1}{\bar{C}}[J^{++} + J^{--}] + \varepsilon \quad , \tag{5.23}$$

where I assumed that $J^{-+} \approx J^{+-}$ because J^{-+} supplies about the same information as J^{+-} (Figure 5.5). Note that the reflector in the following example is strong so it was not necessary to boost the tomographic terms to achieve rapid convergence.

One crucial observation is that J^{+-}, J^{++} and J^{--} all have the same percentage noise because they are all computed by back propagating the same noisy data residuals. Therefore, the proposed boosting will not boost the level of noise. This fact could possibly have been predicted intuitively considering the three terms are resolved by primary reflections with the same signal to noise ratio. By comparison, the signal in the J^{-+} term is a triple scattered wave but the noise in the data is the same so it is inadvisable to boost this term for fear of boosting noise.

5.3.7 Illustration of inversion

Inversion without deeper reflectors

Both of the following examples used a fourth derivative of a Gaussian curve as the source wavelet. This is a narrow-band wavelet that is missing both low and high frequencies. Therefore, there can be no question as to whether or not low wavenumbers present in the inversion solutions result from low frequencies in the source because there are none.

Figure 5.8 shows one of the five shot gathers used in the inversion and generated by finite difference modeling over a circular anomaly embedded in a homogeneous halfspace (Figure 5.9 (a)).

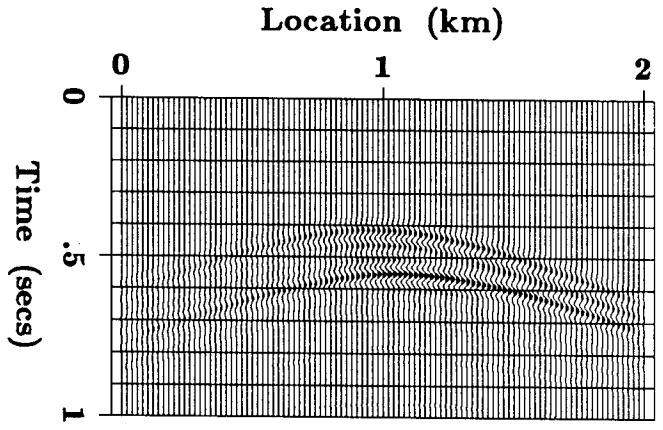

Figure 5.8: Shot gather generated from the model shown in Figure 5.9 (a).

There is *no* deep reflector (i.e. $\bar{C} = 0$ in equation (5.22)) so that the inversion formula given by equation (5.19) implicitly contains only the usual migration-like term (the I^{+-} term). An inversion was performed using a homogeneous starting model. Figures 5.9 (b) and 5.9 (c) shows the inversion result after one and fifteen iterations. The mismatch after

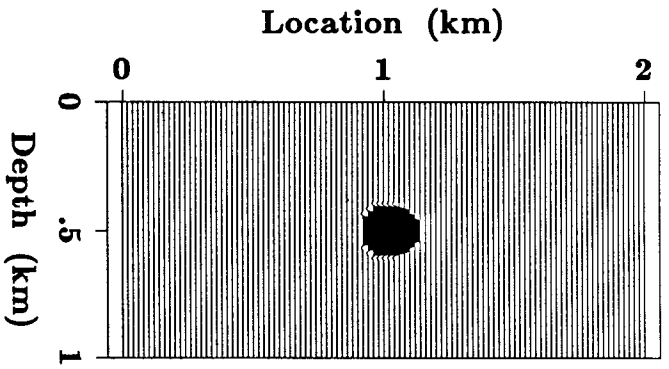

Figure 5.9: (a) True model corresponding to the synthetic data shown in Figure 5.8. Black depicts a negative perturbation and white a positive perturbation relative to the acoustic impedance in the upper layer. The velocity perturbation of the circular region relative to the layer velocity was 10%.

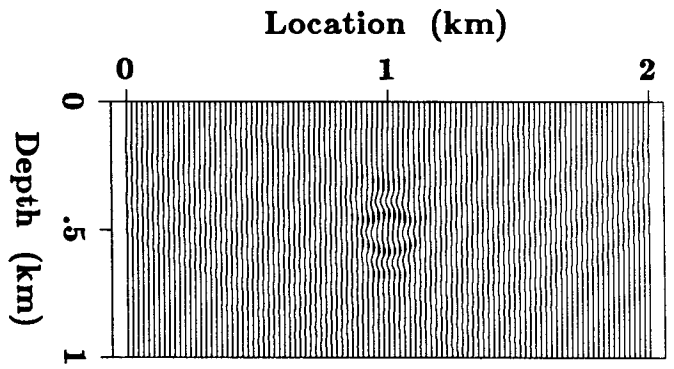

Figure 5.9: (b) One-iteration inversion result plotted as the perturbation relative to the homogeneous starting model.

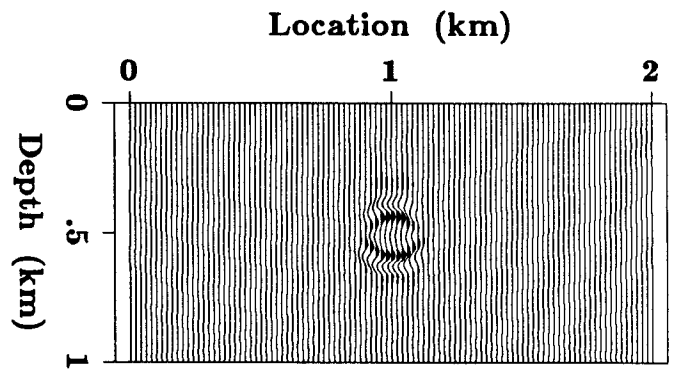

Figure 5.9: (c) Fifteen-iteration inversion result plotted as the perturbation relative to the homogeneous starting model.

fifteen iterations was small (about 12%) so the algorithm has largely, though not completely, converged. The fifteen-iteration result contains only high wavenumbers and looks similar to a migration result (the first-iteration result). This is because the background model was homogeneous and there were no deeper reflectors.

Inversion with deeper reflectors

Now consider the same model but with a strong deeper reflector. The starting model was again homogeneous so the reflector location was *not* assumed to be known a priori. The deep reflector is strong so no boosting of the reflection-tomographic terms was necessary (see the description of boosting after equation (5.22)). One of the five shot gathers used in the inversion is shown in Figure 5.10. The true model and the one- and fifteen-iteration inversion results are in Figures 5.11 (a) through 5.11 (c).

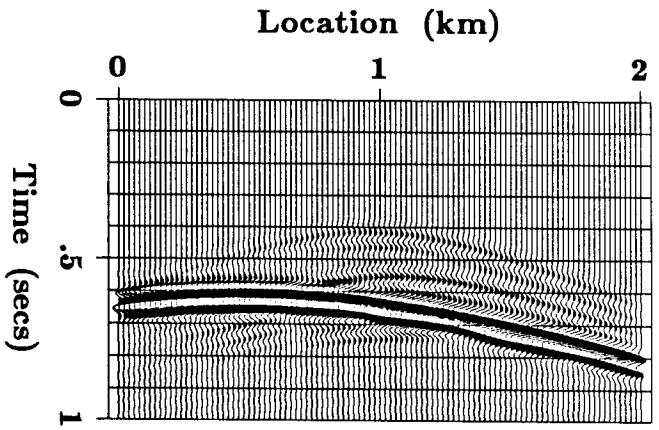

Figure 5.10: Shot gather generated from the model shown in Figure 5.11 (a).

The first-iteration result is the same as in the previous example except that the deeper reflector has been imaged. However, after fifteen iterations, the circular anomaly region, particularly its interval velocity, is better reconstructed and contains both high and low wavenumbers (i.e. both its boundaries and its interval velocity have been found). In other words, the interval velocity inside the circular region is now almost constant and the circular anomaly located by the inversion has almost exactly the same appearance as the true circular anomaly of Figure 5.11 (a). By comparison, the result shown in Figure 5.9 (c) looked like a high pass filtered version of the true anomaly. One reason the anomaly is not more perfectly reconstructed by the inversion is that fifteen iterations were not adequate

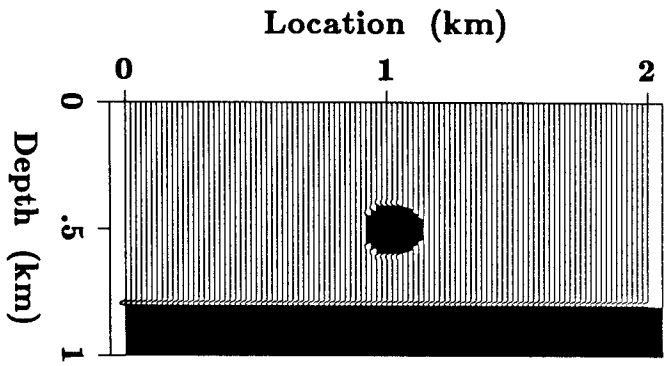

Figure 5.11: (a) True model corresponding to the synthetic data shown in Figure 5.10. Black depicts a negative perturbation and white a positive perturbation relative to the velocity in the upper layer. The velocity perturbation of the circular region relative to the layer velocity was 10%.

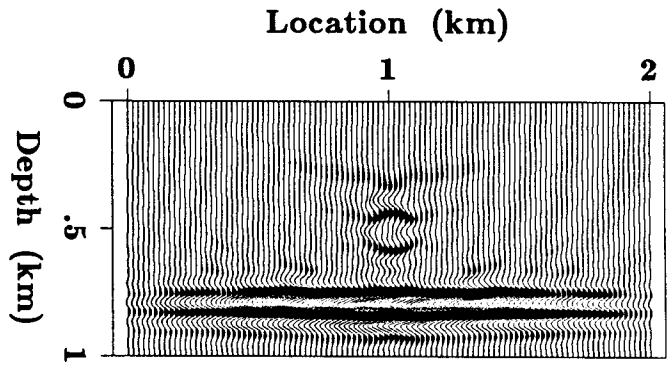

Figure 5.11: (b) One-iteration inversion result plotted as the perturbation relative to the homogeneous starting model.

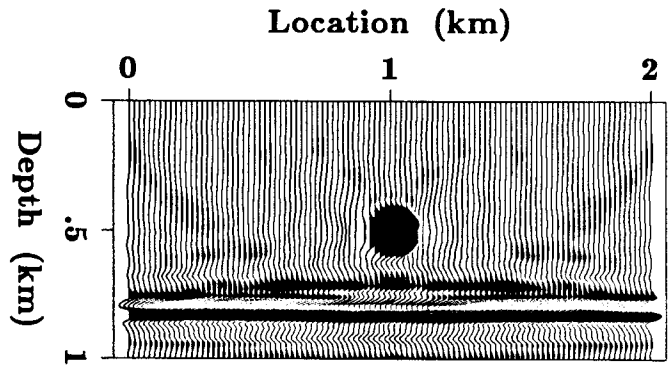

Figure 5.11: (c) Fifteen-iteration inversion result plotted as the perturbation relative to the homogeneous starting model.

for the conjugate gradient algorithm to completely converge. Also, there are small smear artifacts due to the finite number of geophones (101 along the Earth's surface) and sources (five located every 0.5 km starting from 0.0 km).

Discussion

The initial model used in both the above examples was constant and had a velocity equal to that of the upper layer in the true model. Therefore, the first iteration of the inversion was similar to a migration to locate the reflectors. The first example had no deeper reflectors so the three extra inhomogeneous terms did not come into play and only the high wavenumbers could be resolved.

However, the second example had a deeper reflector. Once it was located by the first iteration, the three extra terms (one migration and two reflection tomographic terms) discussed earlier had an effect in the inversion. These helped better reconstruct the underside of the circular region (the I^{-+} term of equation (5.18)) and the interval velocity (the I^{++} and I^{--} terms of equation (5.18)). Subsequent iterations adjusted the velocity model in order to best match the wavefield computed from this model to the "observed" wavefield. Both the reflector location and the interval velocity model were adjusted simultaneously as the iterations proceeded.

5.3.8 Inversion = migration + tomography

The examples illustrate that iterative inversion that updates the velocity model can obtain both high and low wavenumbers in the velocity model. At least two iterations are necessary to solve for the velocities if a smooth velocity model is used as the starting guess (i.e. no a priori knowledge of reflector locations is assumed). The first iteration will locate the reflectors and the second will solve for the interval velocities. Only two iterations are required provided (i) the problem is linear (i.e. there are small velocity perturbations, infinite offsets and Gaussian noise), and (ii) a Newton algorithm rather than a conjugate gradient algorithm is used (i.e. $1/|G|$ is applied). Typically, velocity perturbations are not so small and offsets are finite so the inverse problem is nonlinear. Consequently, more than two iterations are usually required to obtain the complete solution even with a Newton algorithm. Actually, it is often more efficient to use a conjugate gradient method and iterate rather than a Newton method when the velocity model is complex. This is because the inverse Hessian (or equivalently $1/|G|$) required by the Newton algorithm is typically

expensive to compute in comparison to some conjugate gradient iterations. Future research will be required to investigate the utility of the low-wavenumber reflection tomographic terms in the inversion formulas when gradient based inversion schemes are used. This is especially true when many reflectors are present because the boosting factor required by the tomographic terms becomes spatially variable.

The first iteration does an elastic depth migration paying heed to amplitude information and thus locates the reflectors. If the velocity model is not correct, the positioning of reflectors is also not correct. One may ask whether this would unduly affect the inversion. Does the analysis remain valid considering that I assumed the reflector location was exactly known? Would mispositioning of reflectors affect the ability of the algorithm to resolve the low wavenumbers? Since the position of the reflectors is influenced by the initial low-wavenumber velocity model, there is certainly some interaction between the low and high wavenumbers.

Consider a single source and single geophone data. This data cannot resolve between the depth of a reflector and the interval velocity down to that reflector (i.e. if traveltime $t = z/v$ is observed then we cannot differentiate between an increase in velocity v and a decrease in depth z). However, when the data corresponds to an experiment with several sources and geophones, the shapes of the reflection events in the data helps distinguish interval velocity from reflector depth. Also, as the number of illumination angles of waves passing through the layer are increased, the resolution between depth and velocity increases. This is why the example with five sources and 101 geophones converged to a good solution even though the reflector depth was not specified. Hence, I conclude that while the low and high wavenumbers do interact as the iterations proceed, they can be resolved from one another if enough conjugate gradient iterations are performed. The iterations slowly reposition the reflector(s) and update the interval velocities until the solution is obtained.

One further difficulty with inversion schemes is that they may converge to local minima (on the squares error functional that measures the mismatch between observed and synthetic data). This is avoided by starting with a velocity model that is close to the solution. In my experience with seismic inversion, "close" means the initial velocity model must describe the kinematics of wave propagation to within about a half a fundamental wavelength of the seismic source wavelet. An initial inversion step (perhaps interpretive, such as velocity analysis) is still required to obtain this starting velocity model.

The likelihood of a local minima is lessened when doing iterative inversion that vary the

high- and low-wavenumber velocity model. This is because the velocity model can converge on the low wavenumbers from the top of the model down as the iterations proceed. Thus, throughout the iterations there will always be some uppermost portion of the model that obeys the half a wavelength criterion. Consequently, provided the iterations are not too expensive, it may not even be necessary to do the velocity analysis to perform a complete inversion for all wavenumbers. Alternatively, Mora (1987d) suggested how to redefine the objective function to be sensitive to the low wavenumbers and perhaps less nonlinear.

5.4 Conclusions

The elastic inversion formulas derived in Chapter 3 *can find all* wavenumbers in the velocity spectrum (up to some maximum value depending on the maximum frequency in the source) even when the seismic source wavelet is band-limited. In real problems, the inverse solution would still be missing some parts of the wavenumber spectrum of the image because of finite offsets ranges and finite numbers of sources (just like combined velocity analysis and migration).

The inversion is like a combination of iterative migration and reflection tomography. The high wavenumbers (the reflector model) are obtained by migration terms and the low wavenumbers (the layer interval velocities) are found by diffraction tomography terms. Both the reflector model and the interval velocities are obtained simultaneously and automatically in iterative wave equation inversion schemes.

The low wavenumbers can be reconstructed by my iterative elastic inversion scheme so this method should constitute a "complete" inversion obtaining all resolvable wavenumbers in the spectra of the elastic parameters. On a powerful computer such as a CRAY-3, or highly parallel computer such as a Connection Machine (Hillis, 1986), these methods may one day overtake in utility the efficient but partial solutions of velocity analysis and migration.